Axially Chiral Cannabinoids: Design, Synthesis, and Cannabinoid Receptor Affinity

Sara E. Kearney[1], Anghelo J. Gangano[1], Primali V. Navaratne[1], Daniel G. Barrus[3], Kyle J. Rehrauer[2], Terry-Elinor R. Reid[2], Adrian Roitberg[1] Ion Ghiviriga[1], Christopher W. Cunningham*,[2] Thomas Gamage* [3], and Alexander J. Grenning[1]*

[1]Department of Chemistry, University of Florida, PO Box 117200 Gainesville, FL

[2]Concorida University Wisconsin School of Pharmacy, Mequon, WI

[3]Center for Drug Discovery, RTI International, Research Triangle Park, NC

Supporting Information Placeholder

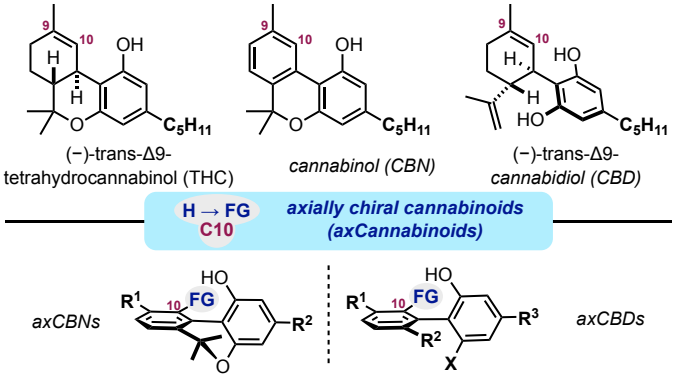

ABSTRACT: The resorcinol-terpene phytocannabinoid template is a privileged scaffold for the development of diverse therapeutics targeting the endocannabinoid system. Axially chiral cannabinols (*ax*CBNs) are unnatural cannabinols (CBNs) that bear an additional C10 substituent, which twists the cannabinol biaryl framework out of planarity creating an axis of chirality. This "escape from flatland" is hypothesized to enhance both the physical and biological properties of cannabinoid ligands, thus ushering in the next generation of endocannabinoid system chemical probes and cannabinoid-inspired leads for drug development. In this full report, we describe the philosophy guiding the design of *ax*CBNs as well as several synthetic strategies for their construction. We also introduce a second class of axially chiral cannabinoids inspired by cannabidiol (CBD), termed axially chiral cannabidiols (*ax*CBDs). Finally, we provide an analysis of axially chiral cannabinoid (*ax*Cannabinoid) atropisomerism, which spans two classes (class 1 and 3 atropisomers), and provide first evidence that *ax*Cannabinoids retain—and in some cases, strengthen—affinity and functional activity at cannabinoid receptors. Together, these findings present a promising new direction for the design of novel cannabinoid ligands for drug discovery and exploration of the complex endocannabinoid system.

INTRODUCTION

Phytocannabinoids and their synthetic analogs are prime candidates for pharmaceutical innovation in the quest for alternatives to highly addictive opioid analgesics, though they have yet to achieve FDA approval for this formidable goal.[1,2] More generally, cannabinoid-based chemical probes and leads are essential for continued exploration of the endocannabinoid system, a complex neuro- and immunomodulating network implicated in a variety of neurodegenerative diseases as well as inflammation, metabolic disorders, and cancer.[1,3] Most phytocannabinoid research to date has focused on the natural *trans*-tetrahydrocannabinol (*trans*-THC) and cannabidiol (CBD) frameworks, which has led to several approved medications (Figure 1A).[4–11] For example, (–)-trans-Δ^9-THC is FDA approved (Dronabinol) for the treatment of HIV/AIDS-induced anorexia[12] as well as chemotherapy-induced nausea and vomiting.[13] The approval of CBD (Epidiolex®) to treat refractory childhood seizures marked the first time a *cannabis*-derived product was approved by the FDA.[14] Synthetic cannabinoids inspired by THC have emerged due to well-established synthetic protocols dating back to the 1940s via a renaissance of research in the late 20th century.[15] Additionally, there are numerous inspiring routes to CBD[16] and minor cannabinoids.[17] In this regard, Nabilone is approved to treat chemotherapy-induced nausea and vomiting,[18] and Ajulemic acid has reached various clinical trial phases as a treatment for systemic sclerosis, dermatomyositis, cystic fibrosis, and systemic lupus erythematosus (Figure 1B).[19] Beyond the THC scaffold, other frameworks for synthetic cannabinoids have appeared, including cyclohexylphenols (e.g., CP55,940),[20] cannabidiol derivatives (e.g., KLS-13019),[21] cannabilactones (e.g., AM1714),[22] and a variety of other heterocyclic scaffolds described elsewhere.[23]

Recently, we proposed that axially chiral analogs of cannabinoids may serve as valuable tools and leads for cannabinoid-based drug discovery (*ax*Cannabinoids, Figure 1C).[24] Scaffolds of this type are attractive for the following reasons: (i.) *ax*Cannabinoids are three-dimensional ligands (due to axial chirality rather than the *trans*-point chirality of *trans*-THCs).[25,26] It is well understood that three-dimensional ligands can exhibit superior recognition for their biological targets compared to planar analogs.[27–29] (ii.) They are built upon a central biaryl framework. Biaryls are readily functionalized by numerous methods and are often metabolically stable. These features have

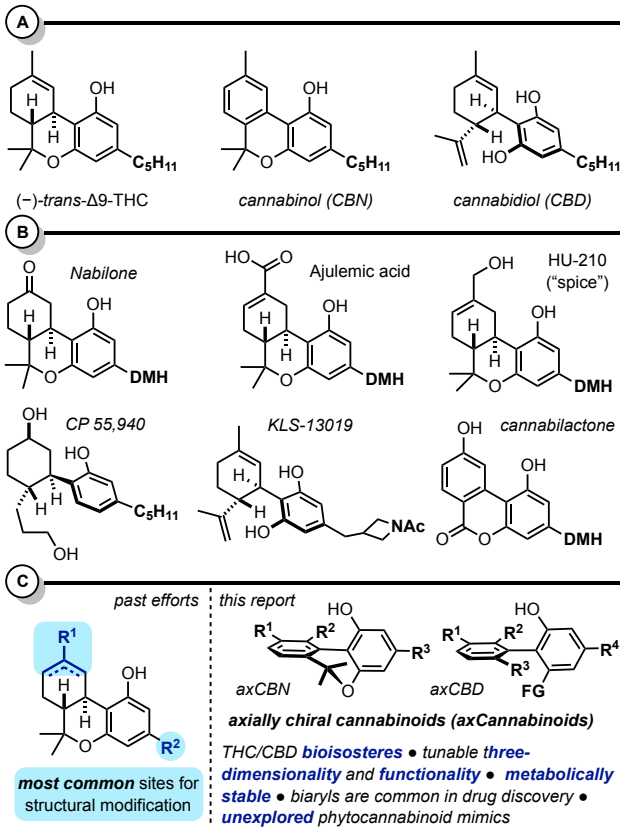

Figure 1. A: *The major phytocannabinoids (THC, CBN, and CBD).* ***B:*** *Representative synthetic cannabinoids.* ***C:*** *Past efforts and this work: axCannabinoids as bioisosteric variants with improved physical and biological properties.*

made biaryls a common template in drug discovery campaigns.[30] This quality is particularly relevant to cannabinoid design as many phytocannabinoids and synthetic variants are prone to aerobic and metabolic oxidation.[31] (iii.) Axial chirality is unexplored with respect to cannabinoid ligands, providing potentially rich grounds for discovery and innovation. In this report, we describe our initial efforts to establish *ax*Cannabinoids as valuable lead molecules with high affinity for cannabinoid receptors. We describe the synthetic chemistry for accessing axially chiral cannabinols (*ax*CBNs), introduce axially chiral cannabidiols (*ax*CBDs), and disclose the results of affinity studies for select *ax*Cannabinoids at the cannabinoid receptors (hCB1R and hCB2R).

RESULTS AND DISCUSSION

Synthetic methods toward axially chiral cannabinols (*ax*CBNs).

We previously reported a scalable, first-generation synthesis of "parent" axially chiral cannabinol (*ax*CBN), the C9-to-C10 methyl-transposed isomer of cannabinol (CBN) (Figure 2A).[12] By design, this transposition results in significant topological changes to the cannabinoid architecture: the ground state biaryl dihedral angle increases from 19° in CBN to 38° in *ax*CBN. CBNs are relatively planar with little barrier to inversion, whereas *ax*CBNs have significant three-dimensionality with barriers to atropisomersim ranging from 14 – 17 kcal/mol (class 1 atropisomerisim).[32] Retrosynthetically, we envisaged access to *ax*CBN via an intramolecular Diels-Alder approach to biaryls (DAB).[33–35] This revealed dimethylpropargyl chloride **1**, allylcyanide **2**, and the olivetol derivative **3** as potential starting materials. A successful route to *ax*CBN and other C10-substituted analogs was achieved through a key biaryllactone intermediate **7** (Figure 2B). This advanced scaffold was prepared via Cu-catalyzed dimethylpropargylation between **1** and **3** (yielding **4**), $TiCl_4$ / Et_3N-promoted condensation between **4** and allylcyanide **2** (yielding an inseparable mixture of *E*-**5** and *Z*-**5**), intramolecular Diels-Alder cycloaddition (yielding **6**), DDQ oxidation, and demethylative Pinner reaction (yielding **7**). ***ax*CBN-1** was prepared via $LiAlH_4$ reduction (Figure 2B) and "parent" ***ax*CBN** was prepared in two additional steps.

While this initial synthetic strategy provided ample amounts of parent ***ax*CBN** and ***ax*CBN-1** over a reasonably efficient synthetic sequence (6 – 8 steps from **1, 2**, and **3**), it is not without shortcomings. Synthetic challenges include a non-selective vinylogous aldol condensation that produces an inseparable mixture of *E*-**5** and *Z*-**5**, and only the Z isomer reacts as desired in the subsequent step. As shown in Figure 2C, the *E*-**5** isomer undergoes a propargyl Claisen rearrangement to benzochromene **8**. More significantly, our goal of preparing diverse

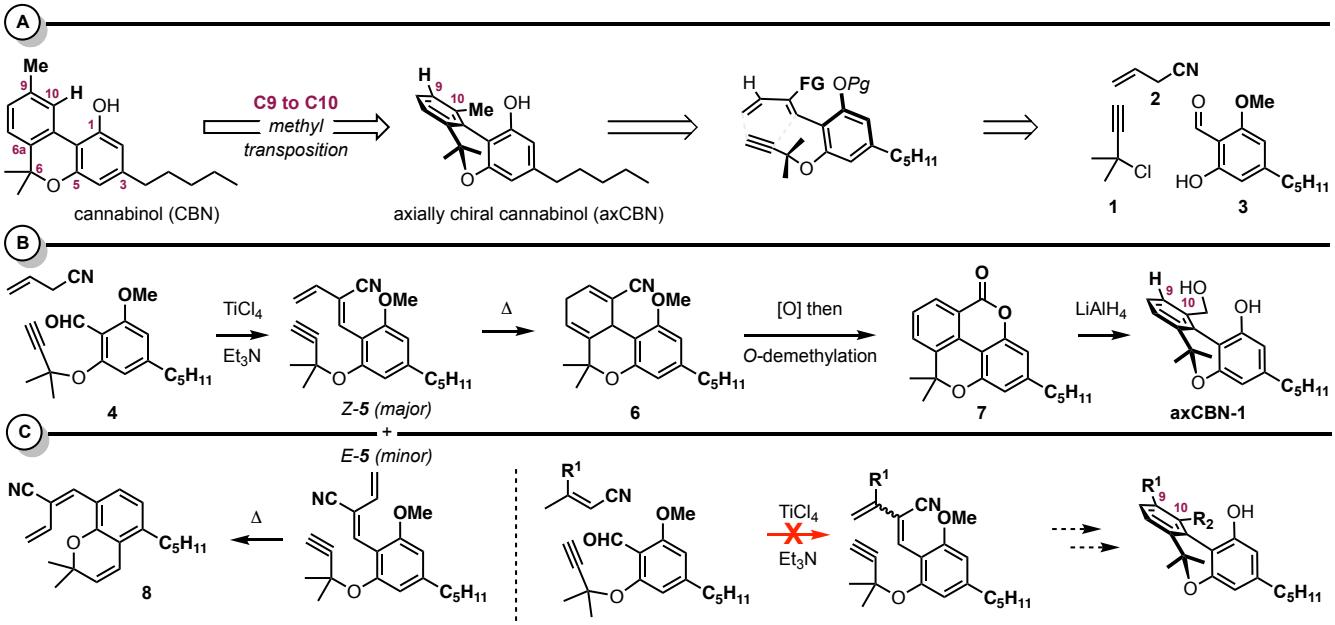

Figure 2. *axCBN retrosynthesis* ***(A)****, forward synthesis* ***(B)****, and representative synthetic shortcomings* ***(C).***

analogs with variable C9-substitution was thwarted as the key $TiCl_4$ / Et_3N-promoted condensation between substituted crotonitriles (R ≠ H) was unsuccessful (Figure 2C).

The issues we encountered during our initial studies (Figure 2C) prompted us to explore an alternative protocol for accessing *ax*CBNs bearing both C9 and C10 substitution, as we hypothesized that the most active *ax*CBN analogs would have substituents at both positions. Simple transposition of the C9 methyl group to the C10 position generates a "methyl void" on the parent scaffold, and methyl groups are known to have significant impact on drug properties (the "magic methyl effect").[36] Consequently, deletion of the C9 methyl substituent may negatively impact the affinity and efficacy at cannabinoid receptors. Thus, we aimed to develop a synthetic route capable of facilitating diverse C9 and C10 substitution as well as variation at other positions. In this regard, we envisioned access to *ax*CBN analogs from **12** by a sequential intramolecular aldol condensation / Diels-Alder cycloaddition yielding the advanced

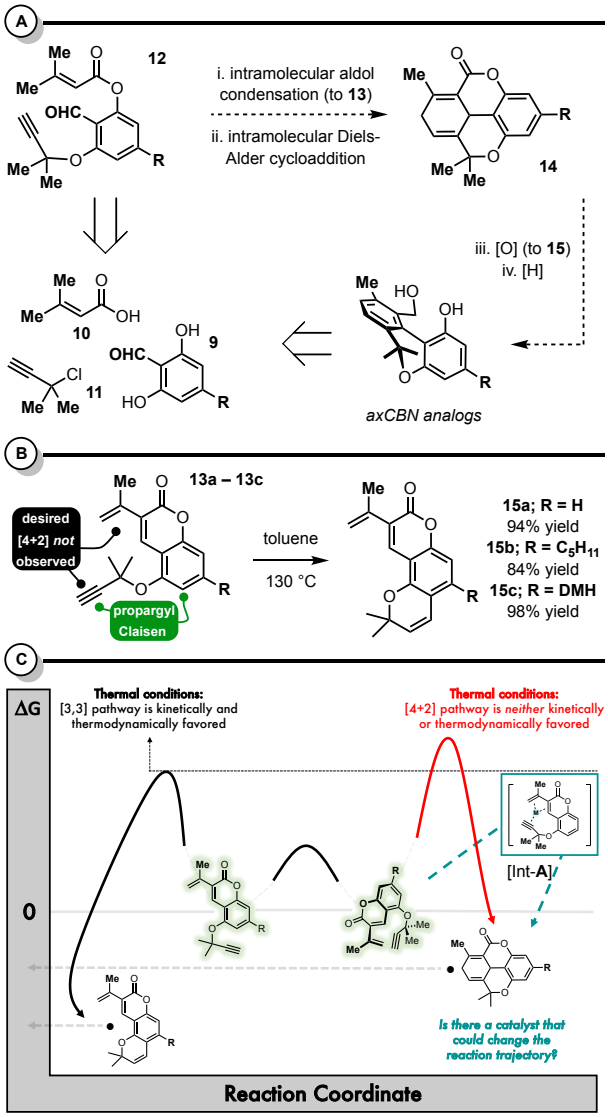

Scheme 1. *A: 2nd-generation strategy capable of achieving C9 and C10 disubstitution. B: Diels-Alder cycloaddition is no longer favorable over propargyl Claisen rearrangement. C: Can the innate [3,3] reactivity be overturned in favor of dearomative [4+2] cycloaddition?*

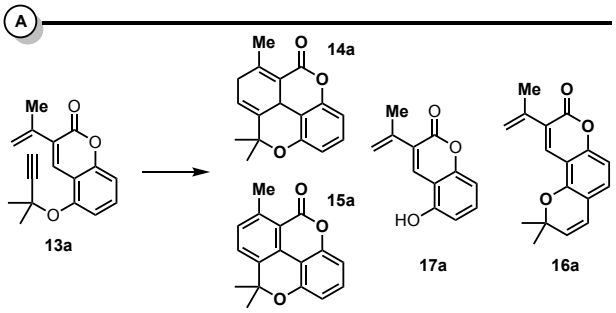

entry	catalyst (10 mol%)	additive (10 mol%)	solvent (0.5 M)	temp (°C)	conv. (%)	14a (% yield)	15b (% yield)	17a (% yield)	16a (% yield)
1	$Rh(PPh_3)_3Cl$	–	TFE	55	100%	10%	9%	3%	29%
2	$Rh(PPh_3)_3Cl$	Ag(OTf)	TFE	55	100%	32%	20%	–	–
3	$Rh[(nbd)Cl]_2$	$AgSbF_6$	TFE	rt	100%	38%	–	23%	–
4	$Rh[(nbd)Cl]_2$	Ag(OTf)	TFE	rt	100%	12%	15%	28%	–
5	$Rh[(nbd)Cl]_2$	$AgBF_4$	TFE	rt	100%	4%	33%	–	–
6	$Rh[(cod)Cl]_2$	$AgSbF_6$	TFE	rt	100%	68%	–	13%	–
7	$Rh[(cod)Cl]_2$	Ag(OTf)	TFE	rt	100%	40%	42%	–	–
8	$Rh[(cod)Cl]_2$	$AgBF_4$	TFE	rt	100%	57%	14%	–	–
9	–	–	TFE	55	10%	–	–	–	~10%

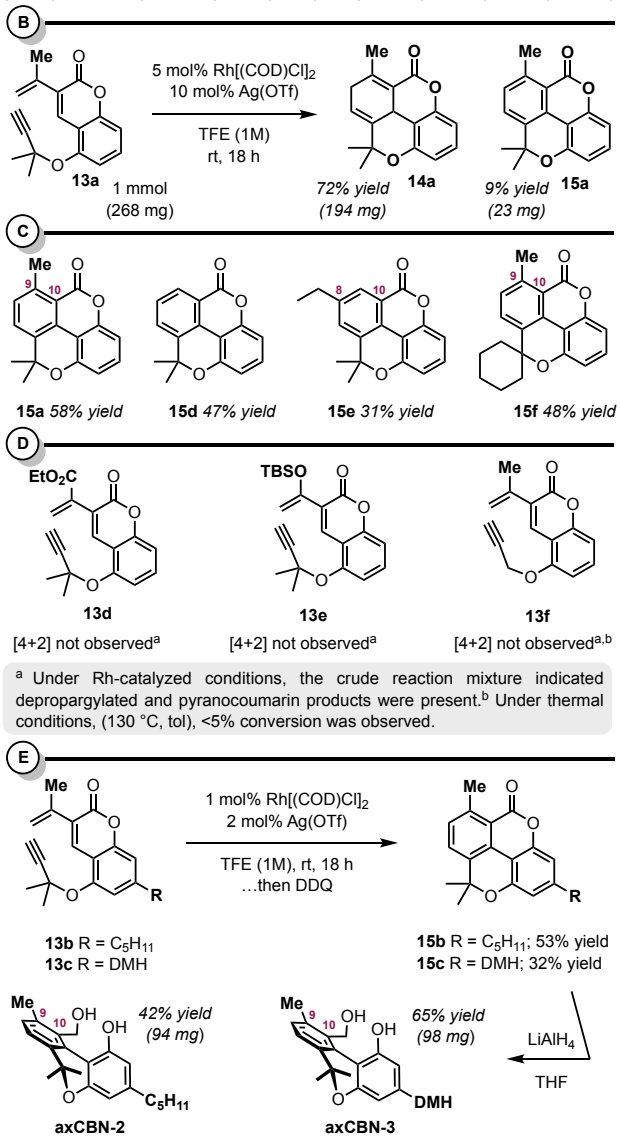

[a] Under Rh-catalyzed conditions, the crude reaction mixture indicated depropargylated and pyranocoumarin products were present.[b] Under thermal conditions, (130 °C, tol), <5% conversion was observed.

Scheme 2. *Optimization* ***(A)*** *and scalability* ***(B)****, Scope* ***(C)****, and limitations* ***(D)*** *of Rh-catalyzed dearomative [4+2] cycloaddition.* ***E.*** *Synthesis of axCBN-2 and axCBN-3.*

tetracyclic intermediate **14** (Scheme 1A). Upon cyclohexadiene oxidation and biaryl lactone ring opening, *ax*CBN analogs would be unveiled. We postulated that the key scaffold **12** could be prepared simply from the requisite olivetol-aldehyde **9**, 3,3-dimethylacrylic acid **10**, and dimethylpropargyl chloride **1**, with known literature procedures for preparing aryl dimethylpropargyl ethers[37–40] and divinylcoumarins serving as inspiration.[40,41]

At the outset of our studies, we successfully prepared model Diels-Alder precursors **13a – 13c** by the proposed Cu-catalyzed dimethylpropargyl ether synthesis, phenol acylation with 3,3-dimethylacrylic acid **10**, and intramolecular vinylogous aldol condensation (Scheme 1B). At this point, we realized that the desired thermal [4+2] transformation would be more challenging than we initially anticipated: under thermal conditions, these substrates exclusively react via propargyl Claisen rearrangement to yield pyranocoumarins.[42,43] It became apparent that a critical Curtin-Hammett kinetics challenge exists in which the desired product **14** is neither thermodynamically nor kinetically favored over the propargyl Claisen rearrangement (Scheme 1C). Recall from Figure 2 that the *Z*-cyano-1,3-diene underwent *favorable* [4+2] cycloaddition over propargyl Claisen rearrangement. While **13** has the correct 1,3-diene geometry, the kinetics and thermodynamics of the desired [4+2] cycloaddition are less favorable due to the aromaticity of the coumarin (which must be broken during the Diels-Alder reaction).[40,44,45] Thus, to achieve the desired transformation, reversal of the innate Curtin-Hammett controlled reactivity is necessary. Toward this goal, we envisioned that a transition-metal catalyst could template the diene and dienophile (via intermediate-**A** (Int-**A**); Scheme 1C), resulting in an altered kinetic profile and mechanism favoring formation of the coumarin-dearomatized [4+2] product (Figure 2). While there are many examples of metal catalyzed [4+2] cycloisomerization,[46–53] vinylcoumarins as dienes, dearomatization, and Curtin-Hammett kinetics challenges are novel to this research area.

To achieve the desired [4+2] reactivity, rhodium(I) catalysis was examined (Scheme 2A).[48,50,52,53] Using Wilkinson's catalyst, $(PPh_3)_3RhCl$, in trifluoroethanol (entry 1), we observed a complex mixture of products that notably contained the desired [4+2] cycloadduct **14a** and its oxidation product, biaryl **15a**. Also observed was the depropargylated product **17a** and the propargyl Claisen rearrangement product **16a**. The addition of catalytic Ag(OTf) improved the result to 32% yield **14a** and 20% yield **15a** (entry 2). Catalytic $[Rh(NBD)Cl]_2$/Ag(I) additives performed comparably to Wilkson's catalyst / Ag(OTf) (entries 3 – 5 *versus* entry 2). The best results were achieved with catalytic $[Rh(COD)Cl]_2$ / Ag(I) salts in trifluoroethanol (entries 6 – 8) where combined 68% – 82% yields of **14a** and **15a** were obtained. Notably, the reaction performed similarly well on the 1 mmol scale (Scheme 2B). As a control, we examined the reaction catalyst-free in trifluoroethanol (entry 9), confirming the essential impact of the catalyst. We briefly examined general substitution patterns (Scheme 2C – 3E), targeting the tetracyclic scaffolds **15a – 15f** directly via a one-pot, two-step Rh(I)-catalyzed [4+2] cycloaddition followed by in situ DDQ oxidation of the resulting 1,4-cyclohexadienes to the corresponding arenes (Scheme 2C and 2E).[54] Products **15d** and **15e** represent variations in the diene component. Unsubstituted (**15d**) and ethyl substituted (**15e**) dienes were reasonably tolerated. In contrast, modifications to the diene electronics resulted in little to no sign of the desired products (Scheme 2D). For example, ester substrate **13d** and the silyl–enol ether diene **13e** were not competent Diels-Alder substrates. With respect to the propargylic substitution on the dienophile, a cyclohexyl group was tolerated yielding **15f**. However, in the absence of substitution, the transformation did not occur (Scheme 2D, **13f**).

The scope studies related to the Rh(I)-catalyzed [4+2] cycloaddition suggest that a variety of C8 / C10 (**15e**) and C9 / C10 (**15a** and **15f**) disubstituted *ax*CBNs can be accessed. Along these lines, coumarins **13b** and **13c** bearing the common cannabinoid aliphatic chains (pentyl and dimethylheptyl (DMH), respectively) on the resorcinol-portion of the scaffold were prepared. Gratifyingly, the Rh(I)-catalyzed [4+2] cycloaddition/oxidation sequence yielded the desired pyrano-biaryllactones **15b** and **15c.** $LiAlH_4$ reduction furnished the targeted *ax*CBN analogs, ***ax*CBN-2** and ***ax*CBN-3**.

Synthetic methods toward axially chiral cannabidiols (axCBDs).

During our studies related to the first-generation route to *ax*CBNs (Figure 2), specifically, the attempted demethylation to free the phenol on **6**, we encountered a transformation that converted the Diels-Alder adduct **6a** into the biaryl **18a** with concomitant pyran ring cleavage (Scheme 3). We surmised that this transformation occurred by an "$E1_{cb}$ aromatization." In this process, the nitrile group directs deprotonation yielding int-**B**, which is poised for pyran ring-cleavage to phenoxide int-**C**. In-situ or upon acidic work up, int-**C** undergoes a thermodynamically favorable isomerization from the nonaromatic isotoluene to the biaryl product **18.** This was an interesting outcome as it resulted in an axially chiral biaryl by a unique method, and the structure is reminiscent of the theoretical "parent" axially chiral cannabidiol (*ax*CBD). Regarding the method, Diels-Alder reaction between dienes and alkynes to yield arenes usually relies on oxidation of the intermediate 1,4-cyclohexadiene[45,55] or elimination of an endocyclic leaving group.[56,57] Thus, this represents a unique strategy for targeting substituted and functionalized arenes. With respect to CBD, *ax*CBD is formulated in analogy to the relationship between THC and *ax*CBN: the cyclohexene ring of the parent natural product is formally oxidized to the arene, and the methyl group is transposed from the C9 to the C10 position, thus resulting in axially chiral cannabidiols. This term should be considered loosely as parent *ax*CBD is *prochiral*

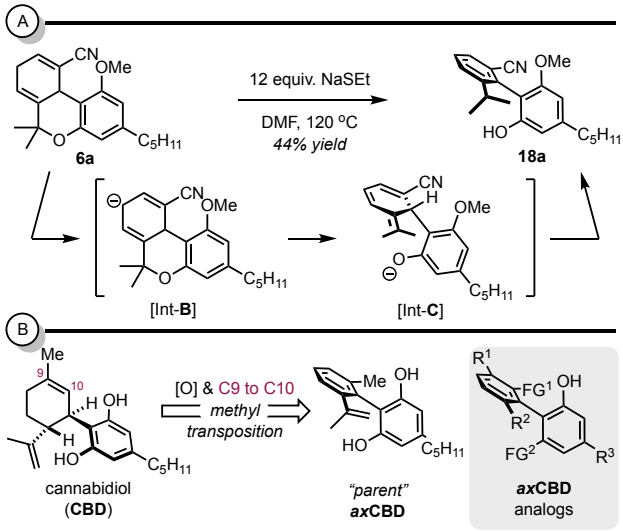

***Scheme 3. A:** Observation of an $E1_{cb}$ elimination reaction yielding a biaryl reminiscent of parent axCBD. **B:** Cannabidiol (CBD) and axially chiral cannabidiol (axCBD).*

rather than chiral, but it bears an orthogonal, conformationally restricted biaryl linkage and thus is three-dimensional. That said, many *ax*CBD *analogs* have the potential to be axially chiral biaryls.

Intrigued by the initial result and the potential to mimic the structure of cannabidiol (CBD) with axially chiral analogs, we designed a model substrate to optimize the $E1_{cb}$ aromatization sequence for targeting *ax*CBDs (Scheme 4). The key substrates (**6a – 6i**) were prepared by the same synthetic sequence outlined in Figure 2: (i.) $TiCl_4$ / Et_3N-mediated aldol condensation between allyl cyanide and the requisite O-dimethylpropargylsalicylaldehyde then (ii.) intramolecular Diels-Alder cycloaddition. It was found that various bases could instigate the $E1_{cb}$ aromatization, but LiHMDS was optimal (see the supporting information for select optimization reactions). This reaction can be performed on the gram scale, and a variety of unique *o*-benzonitrile– *o*'-phenol biaryls were prepared in good yields under the optimized protocol. Notably, halogen functional handles are tolerated at every position about the phenol (**18c – 18g),** and an *o*-benzonitrile-*o*'-naphthol biaryl **18h** is accessible. With the goal of applying this method to the synthesis of *ax*CBD analogs, Diels-Alder adducts **6a** and **6i** were accessed on the 0.5 – 1 gram scale. Under the standard $E1_{cb}$ aromatization conditions, we prepared the advanced axially chiral biaryl intermediates **18a** and **18i** in good yields (54% and 44%, respectively). Nitrile reduction to the alcohol was achieved via sequential addition of DIBALH and $NaBH_4$ yielding ***ax*CBD-1** (R = pentyl) and ***ax*CBD-2** (R = dimethylheptyl (DMH)).

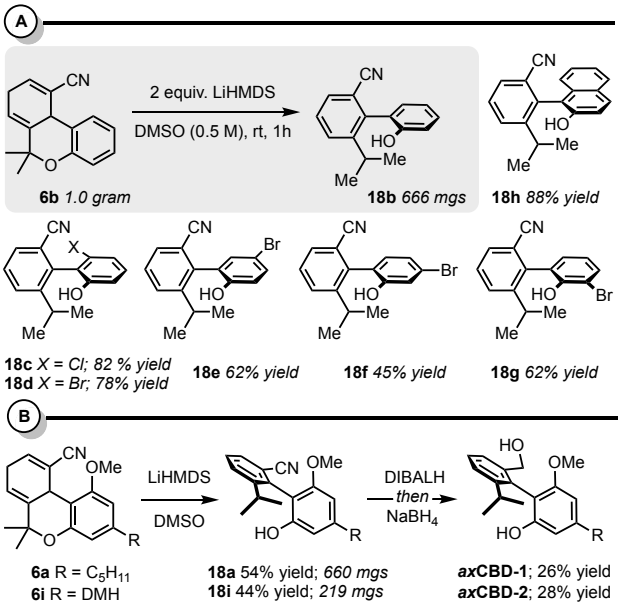

***Scheme 4. A:** Biaryl synthesis via $E1_{cb}$ aromatization: Scalability and scope studies. **B:** Synthesis of **axCBD-1** and **axCBD-2** utilizing $E1_{cb}$ aromatization*

Atropisomerism of axially chiral cannabinoids

Axially chiral cannabinols (*ax*CBNs) and cannabidiols (*ax*CBDs) differ from their respective natural product counterparts, THC and CBD, by oxidation of the natural cyclohexene to a benzene ring and C9 to C10 methyl transposition. These molecules are biaryl but *three-dimensional* in the ground state. Using VT-NMR, we determined the barrier to atropisomerism for ***ax*CBN-2** and its *bis*-acetate, ***ax*CBN-4**, to be 14 kcal/mol and 17 kcal/mol, respectively (Scheme 5). Regarding *ax*CBDs, VT-NMR experiments indicated that the biaryl linkage was conformationally stable: no coalescence of the enantiotopic signals was observed up to 95 °C in toluene-D_8. These studies revealed that we have synthesized two classes of axially chiral cannabinoid thus far:[25] *ax*CBNs are class 1 atropisomers while *ax*CBDs are class 3 atropisomers. Regarding *ax*CBNs, they are three-dimensional in their ground state (biaryl dihedral angle = 38°), but rapidly equilibrating. Thus, both enantiomeric conformers are accessible under ambient conditions.

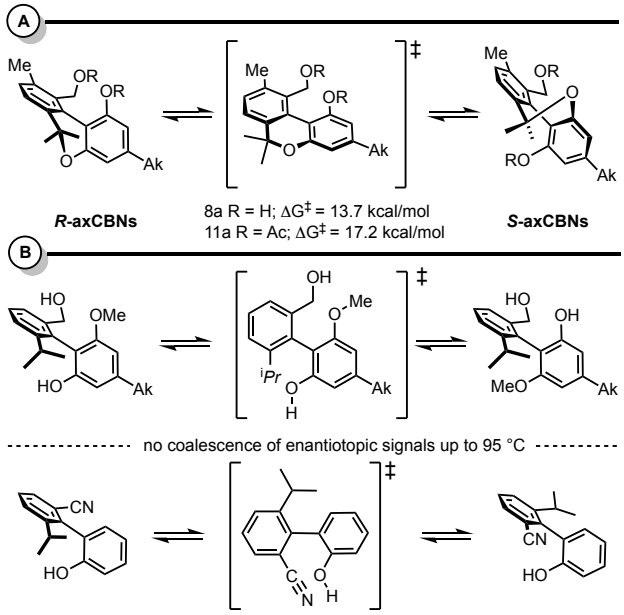

***Scheme 5. A:** axCBNs display "type 1" atropisomerism. **B:** axCBDs display "type 3" atropisomerism.*

Molecular pharmacology of axial chiral cannabinoids at cannabinoid receptors.

We have examined a small series of *ax*Cannabinoids for binding affinity and functional activity at human cannabinoid receptors (hCB1R and hCB2R) (Scheme 6 and 7). From this initial series, several compounds emerged with desirable pharmacology relative to the relevant parent phytocannabinoid in terms of affinity and selectivity. ***ax*CBN-3** exhibited sub-nanomolar affinity for both receptors, approximately 360-fold higher than CBN at hCB1R and 134-fold higher at hCB2R.[58] When compared to the dimethylheptyl derivative of CBN (CBN-DMH) reported by Rhee and coworkers,[58,59] ***ax*CBN-3** has approximately 5-10-fold higher affinity. This suggests that the addition of the C-10 group, which biases the biaryl to a nonplanar configuration, confers additional beneficial interactions with hCB1R and hCB2R that result in higher affinity. Notably, axCBN-3 demonstrated higher affinity than the positive control, CP55,940, at both receptors.[58] Additionally, ***ax*CBD-2** and ***ax*CBN-4** exhibited increased selectivity for hCB2R, 4.8- and 6.2-fold, respectively.

Importantly, these compounds maintained functional activity as determined by stimulation of [^{35}S]GTPγS binding, an assay of native G protein activation (Supplementary Tables 4 and 5). ***ax*CBN-3** exhibited an 8-fold greater potency to stimulate [^{35}S]GTPγS binding at hCB2R than at hCB1R while exhibiting increased efficacy over CBN. ***ax*CBN-4** also maintained agonist activity at hCB2R. Notably, ***ax*CBD-2** exhibited 7.4-

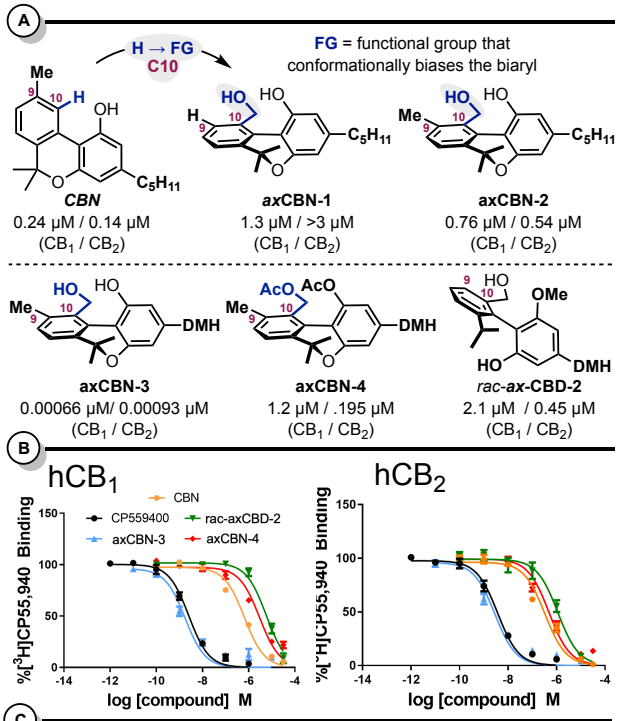

C

	hCB1R		hCB2R		
	pKi ± SEM	Ki (nM)	pKi ± SEM	Ki (nM)	CB1/CB2
CP55,940	9.03 ± 0.0292	0.933	8.86 ± 0.107	1.38	0.7
CBN	6.62 ± 0.0627	240	6.86 ± 0.0370	138	1.7
CBD	5.48 ± 0.0605	3310	5.85 ± 0.0374	1410	2.3
axCBD-2	5.67 ± 0.0821	2140	6.35 ± 0.0755	447	4.8
axCBN-3	9.18 ± 0.0794	0.661	9.03 ± 0.141	0.933	0.7
axCBN-4	5.92 ± 0.125	1200	6.71 ± 0.122	195	6.2

D

	hCB1R		hCB2R	
	pEC_{50}	E_{max}	pEC_{50}	E_{max}
CP55,940	9.09 ± 0.476	0.0913 ± 0.0173	9.17 ± 0.108	0.121 ± 0.0298
axCBN-3	7.58 ± 0.763	0.0807 ± 0.0141	8.46 ± 0.182	0.120 ± 0.0296
axCBN4	5.15 ± 0.954	0.175 ± 0.0832	6.75 ± 0.397	0.120 ± 0.0294
axCBD-2	NA	NA	7.54 ± 0.381	0.0839 ± 0.0176

Values reflect mean±SEM of an least N=3 experiments performed in triplicate.
NA = no observable agonism at concentrations up to 31.6 μM

Figure 6. A: *axCannabinoid summary.* ***B:*** *Displacement of [3H]CP55,940 binding.* ***C:*** *axCannabinoid binding affinity at cannabinoid receptors.* ***D:*** *Functional effects of axCannabinoids in Gai1 activation.*

fold greater potency in [35S]GTPγS binding. Further, ***ax*CBD-2** exhibited agonism at hCB2R in the TRUPATH assay of Gαi1β3γ9 protein activation (Supplementary Tables 6 and 7), but not at hCB1R at concentrations up to 31.6 μM (Figure 6D), suggesting a potential route for development of selective hCB2R agonists. This functional activity diverges from that of the parent CBD which exhibits no efficacy at either cannabinoid receptor in either of these assays (data not shown). Interestingly, in contrast to CBN [$F(2, 64) = 1.21$, $p = 0.305$], ***ax*CBN-3** [$F(2, 91) = 42.7$, $p < 0.0001$] exhibited distinct affinities for two binding sites following an extra sum-of-squares F test for one site *versus* two site binding models (Scheme 7). The higher affinity binding may reflect selection for the active conformation, which is also supported by the higher efficacy of ***ax*CBN-3** in [35S]GTPγS binding (Supplementary Tables 4 and 5). Further, because ***ax*CBN-3** is a class 1 atropisomer, it exists as two

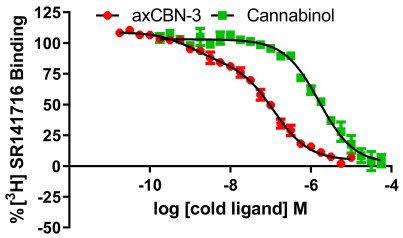

Scheme 7. *axCBN-3 exhibits 2 distinct affinities at hCB1R (pKi_{Hi}=9.4, pKi_{Lo}=7.3), unlike CBN (pKi=6.2), suggesting high affinity binding to the active conformation. Data are mean±SEM of N=3-4 experiments performed in triplicate.*

enantiomeric conformers rapidly equilibrating, each of which may have unique affinities for different conformations and give rise to multiphasic binding curves as depicted in Figure 6. Thus, these compounds may exhibit particularly unique pharmacology in terms of the receptor populations they could stabilize to give rise to unique signaling profiles.

Together, these data showcase that *ax*CBNs and *ax*CBDs can *mimic*—or even *surpass*—the activity of phyto- and synthetic cannabinoids at cannabinoid receptors. These analogs occupy a unique conformational chemical space (ground-state three-dimensional structures), which impacts affinity and selectivity for biological targets (cannabinoid receptors and beyond). These molecules have the potential for improved metabolic and aerobic stability, and they represent a new cannabinoid-based platform for drug discovery and development.

Molecular modeling of axCannabinoids at cannabinoid receptors

We used induced-fit docking (Glide-XP, Schrödinger, Inc.) to predict how *ax*Cannabinoids ***ax*CBN-3** and ***rac-ax*CBD-2** engage hCB1R and hCB2R.[60] The Glide-XP docking scoring function is an approximated binding affinity that is used to rank predicted poses of a ligand as a result of its interaction with a target: ***ax*CBN-3** had an appreciable score with hCB1R (XPgscore -13.285 kcal/mol) and hCB2R (XPgscore -13.711 kcal/mol), and ***rac-ax*CBD-2** had lower predicted affinity in hCB1R (XPgscore -12.488 kcal/mol) compared to hCB2R (XPgscore -13.117 kcal/mol). In each case, the dimethylheptyl tails of the *ax*Cannabinoids occupies the same narrow hydrophobic channel between transmembrane helix (TMH) 3, 5, and 6 as the co-crystalized ligand (Figure 3). Hydrophobic aromatic interactions with Phe268 (hCB1R) and Phe87, Phe94 and Phe183 (hCB2R) are also observed. Canonical structure-activity relationships (SAR) of classical cannabinoids indicate that a free phenol at position 1 is generally required for hCB1R and hCB2R binding.[58] For ***ax*CBN-3**, this group is not predicted to form beneficial interactions with hCB1R, but is predicted to donate a hydrogen bond to Ser285 in hCB2R; the equivalent Ser383 in CB1R does donate a hydrogen bond to the oxygen in the pyran ring. The 10-hydroxymethyl group of ***ax*CBN-3** is predicted to form an intramolecular hydrogen bond (IMHB) with the nearby 1-phenol. This may contribute to target binding by overall lowering the hydrophilicity of this region, allowing this group to occupy an otherwise hydrophobic portion of the binding site. The predicted binding pose of ***rac-ax*CBD-2** differs from that of ***ax*CBN-3** due to the larger dihedral angle connecting the two phenyl rings (ranging from -27.9° to 29.2° for ***ax*CBN-3** and -75.1° to -75.3° for ***rac-ax*CBD-2** when docked in hCB1R and hCB2R, respectively; see Figures S3 – S6 in the

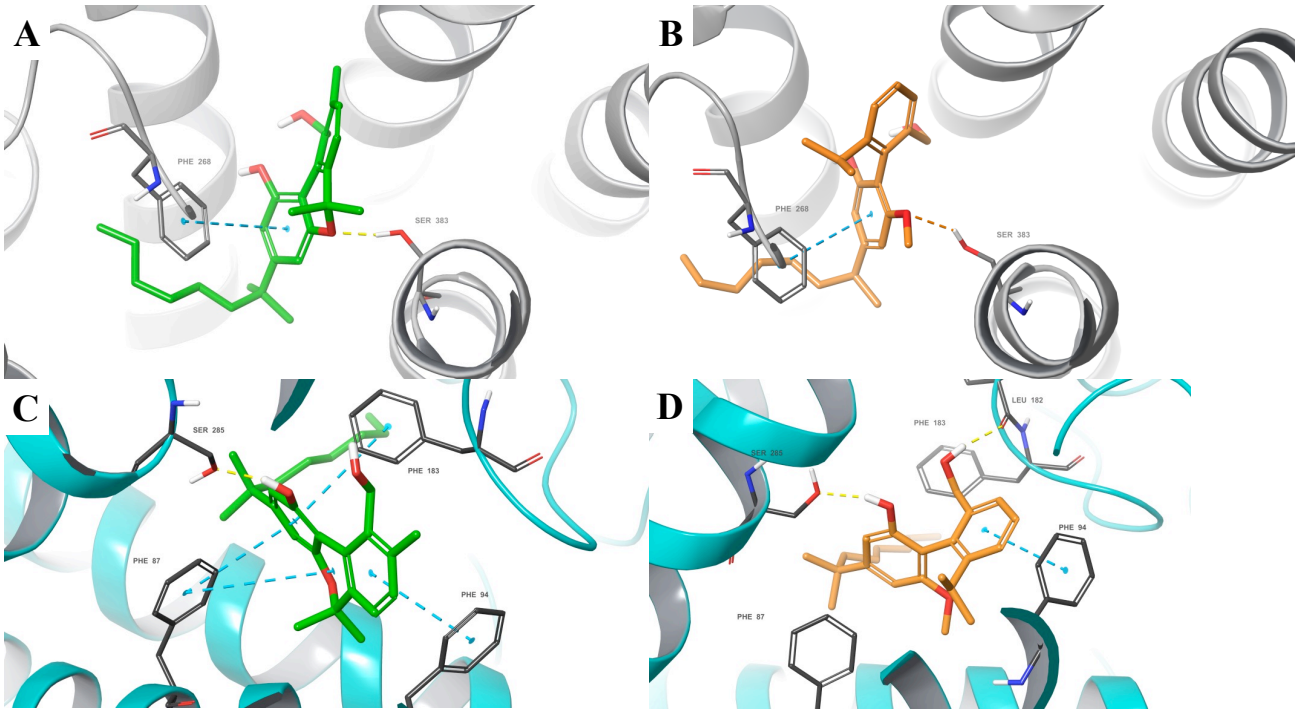

Figure 3. *Results from automated docking. axCBN-3 (green) docked within hCB1R(gray)* ***(A)*** *and hCB2R (green)* ***(B)****, rac-axCBD-2 (orange) docked within hCB1R* ***(C)*** *and hCB2R* ***(D)****. For docking scores, please see the text.*

Supporting Information). Within hCB1R, the 6-propyl substituent points toward Phe268, while the 10-hydroxymethyl group occupies a narrow lipophilic region below the plane of aryl ring A. Multiple steric clashes contribute to a lower Glide score, including a clash with Ser383. Within hCB2R, however, the 10-hydroxymethyl group is able to donate a hydrogen bond to the backbone carbonyl of Leu182, and the phenol forms a beneficial hydrogen bond with Ser285. The presence of these additional beneficial binding interactions may explain the observation that ***rac-ax*CBN-2** is a selective hCB2R agonist.

CONCLUSIONS AND OUTLOOK

We have conceptualized and validated *ax*Cannabinoids as novel leads for cannabinoid-inspired drug discovery. We hypothesize that *ax*Cannabinoids will be uniquely valuable scaffolds due to their three-dimensionality and stability imparted by the central axially chiral biaryl framework. Through the development of various *de novo* synthetic routes and collaborative biological analysis at cannabinoid receptors (hCB1R / hCB2R), we have achieved a preliminary understanding of *ax*Cannabinoid structure-activity relationships. With respect to synthesis, disclosed herein are three distinct synthetic strategies capable of producing diverse analogs bearing either a tricyclic cannabinol framework or a bicyclic scaffold inspired by cannabidiol: axially chiral cannabinols (*ax*CBNs) or cannabidiols (*ax*CBDs), respectively. Numerous products were obtained, including 8 analogs which were examined for biological activity, and we speculate that analogs *beyond* those disclosed herein are accessible with our established protocols. The initial structure-activity relationship study revealed an *ax*Cannabinoid (***ax*CBN-3**) with picomolar affinity for the hCB1 and hCB2 receptors as well as other promising leads (*e.g.* ***ax*CBN-4** and ***rac-ax*CBD-2**) that display >5-fold selectivity for the hCB2 receptor over the hCB1 receptor. The *ax*Cannabinoids described here offer new opportunities to probe the binding sites of cannabinoid receptors and other protein targets of phytocannabinoids. Based on these findings, we plan to (1) further interrogate the biological activity and therapeutic potential of the initial lead molecules, and (2) utilize these findings to design and synthesize the next generation of *ax*Cannabinoids for drug discovery.

It is also worth noting that this strategy of converting point chirality into axial chirality can be applied *beyond* cannabinoids. Many bioactive natural products contain linked 6-membered rings, and we speculate that scaffolds of this type have atropisomeric biaryl bioisosteres that may exhibit improved therapeutic, stability, and other ADMET properties (Figure 4). We propose that this type of structural modification be considered routinely throughout medicinal chemistry campaigns.

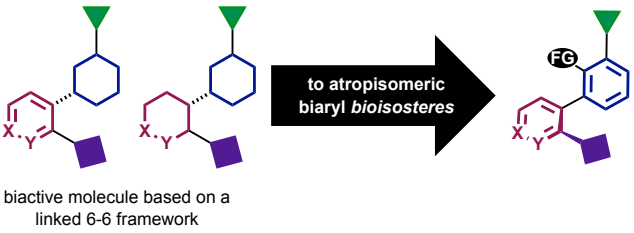

Figure 4. *Beyond cannabinoids: other "lead molecules" in principle can have atropisomeric counterparts with potentially improved pharmaceutical/therapeutic properties.*

ASSOCIATED CONTENT

Supporting Information

Supporting Information includes experimental procedures and characterization data (^{1}H NMR, ^{13}C NMR, HRMS).

AUTHOR INFORMATION

Corresponding Author

*grenning@ufl.edu

Author Contributions

The manuscript was written through contributions of all authors. All authors have given approval to the final version of the manuscript.

ACKNOWLEDGMENT

We gratefully acknowledge the National Institute of General Medical Science (R35 GM137893-01) , the National Center for Complementary and Integrative Health (R01 AT010773), and the National Institute on Drug Abuse (K01 DA045752) for providing support for this research. We thank the Mass Spectrometry Research and Education Center and their funding source: NIH S10 OD021758-01A1.

REFERENCES

(1) Bridgeman, M. B.; Abazia, D. T. Medicinal Cannabis: History, Pharmacology, and Implications for the Acute Care Setting. *P. and T.* **2017**, *42*, 180–188.

(2) Elikottil, J.; Gupta, P.; Gupta, K. The Analgesic Potential of Cannabinoids. *J. Opioid. Manag.* **2009**, *5*, 341.

(3) Scotter, E. L.; Abood, M. E.; Glass, M. The Endocannabinoid System as a Target for the Treatment of Neurodegenerative Disease. *Br. J. Pharmacol.* **2010**, *160*, 480.

(4) Mechoulam, R.; Hanuš, L. A Historical Overview of Chemical Research on Cannabinoids. *Chem. Phys. Lipids.* **2000**, *108*, 1–13.

(5) Ametovski, A.; Lupton, D. W. Enantioselective Total Synthesis of (-)-Δ 9 -Tetrahydrocannabinol via N-Heterocyclic Carbene Catalysis. *Org. Lett.* **2019**, *4*, 1212 – 1215.

(6) Shultz, Z. P.; Lawrence, G. A.; Jacobson, J. M.; Cruz, E. J.; Leahy, J. W. Enantioselective Total Synthesis of Cannabinoids - A Route for Analogue Development. *Org. Lett.* **2018**, *20*, 381–384.

(7) Schafroth, M. A.; Zuccarello, G.; Krautwald, S.; Sarlah, D.; Carreira, Stereodivergent Total Synthesis of Δ9-Tetrahydrocannabinols. *Angew, Chem. Int. Ed.* **2014**, *53*, 13898–13901.

(8) de Vries, M.; van Rijckevorsel, D. C.; Wilder-Smith, O. H.; van Goor, H. Dronabinol and Chronic Pain: Importance of Mechanistic Considerations. *Expert Opin. Pharmacother*. **2014**, *15*, 1525–1534.

(9) Wissel, J.; Haydn, T.; Müller, J.; Brenneis, C.; Berger, T.; Poewe, W.; Schelosky, L. D. Low Dose Treatment with the Synthetic Cannabinoid Nabilone Significantly Reduces Spasticity-Related Pain: A Double-Blind Placebo-Controlled Cross-over Trial. *J. Neurol.* **2006**, *253*, 1337–1341

(10) Nielsen, S.; Germanos, R.; Weier, M.; Pollard, J.; Degenhardt, L.; Hall, W.; Buckley, N.; Farrell, M. The Use of Cannabis and Cannabinoids in Treating Symptoms of Multiple Sclerosis: A Systematic Review of Reviews. *Curr. Neurol. and Neurosci. Rep*. **2018**, *18*.

(11) Abu-Sawwa, R.; Scutt, B.; Park, Y. Emerging Use of Epidiolex (Cannabidiol) in Epilepsy. *J. Pediatr. Pharmacol. Ther.* **2020**, *25*, 485–499.

(12) B, O.; H, M.; V, G. Dronabinol. *Pharma-Kritik.* **2022**, *24*, 29–31. [KE1]

(13) Brafford May, M.; Glode, A. E. Cancer Management and Research Dovepress Dronabinol for Chemotherapy-Induced Nausea and Vomiting Unresponsive to Antiemetics. *Cancer Manag Res* **2016**, *8*, 49–55.

(14) Devinsky, O.; Cross, J. H.; Laux, L.; Marsh, E.; Miller, I.; Nabbout, R.; Scheffer, I. E.; Thiele, E. A.; Wright, S. Trial of Cannabidiol for Drug-Resistant Seizures in the Dravet Syndrome. *N. Engl. J. Med.* **2017**, *376*, 2011–2020.

(15) Bloemendal, V. R. L. J.; van Hest, J. C. M.; Rutjes, F. P. J. T. Synthetic Pathways to Tetrahydrocannabinol (THC): An Overview. *Org. Biomol. Chem.* **2020**, *18*, 3203–3215.

(16) Maiocchi, A.; Barbieri, J.; Fasano, V.; Passarella, D. Stereoselective Synthetic Strategies to (−)-Cannabidiol. *ChemistrySelect.* **2022**, *7*, e202202400.

(17) Dennis, D. G.; Anand, S. D.; Lopez, A. J.; Petrovčič, J.; Das, A.; Sarlah, D. Synthesis of the Cannabimovone and Cannabifuran Class of Minor Phytocannabinoids and Their Anti-Inflammatory Activity. *J. Org. Chem.* **2022**, *87*, 6075–6086.

(18) Davis, M. P. Oral Nabilone Capsules in the Treatment of Chemotherapy-Induced Nausea and Vomiting and Pain. *Expert. Opin. Investig. Drugs.* **2008**, *17*, 85–95.

(19) Burstein, S. H. Ajulemic Acid: Potential Treatment for Chronic Inflammation. *Pharmacol. Res. Perspect.* **2018**, *6*.

(20) Tai, S.; Fantegrossi, W. E. Synthetic Cannabinoids: Pharmacology, Behavioral Effects, and Abuse Potential. *Curr. Addict. Rep.* **2014**, *1*, 129.

(21) Brenneman, D. E.; Petkanas, D.; Kinney, W. A. Pharmacological Comparisons Between Cannabidiol and KLS-13019. *J. Mol. Neurosci.* **2018**, *66*, 121–134.

(22) Liu, Y.; Ho, T. C.; Baradwan, M.; Pascual Lopez-Alberca, M.; Iliopoulos-Tsoutsouvas, C.; Nikas, S. P.; Makriyannis, A. Synthesis of Functionalized Cannabilactones. *Molecules.* **2020**, *25*, 684.

(23) Saldaña-Shumaker, S. L.; Grenning, A. J.; Cunningham, C. W. Modern Approaches to the Development of Synthetic Cannabinoid Receptor Probes. *Pharmacol. Biochem. Behav.* **2021**, *203*, 173119.

(24) Navaratne, P. V.; Wilkerson, J. L.; Ranasinghe, K. D.; Semenova, E.; Felix, J. S.; Ghiviriga, I.; Roitberg, A.; McMahon, L. R.; Grenning, A. J. Axially Chiral Cannabinols: A New Platform for Cannabinoid-Inspired Drug Discovery. *ChemMedChem.* **2020**, *15*, 728–732.

(25) Toenjes, S. T.; Gustafson, J. L. Atropisomerism in Medicinal Chemistry: Challenges and Opportunities. *Future. Med. Chem*. **2018**, 409–422.

(26) Smith, D. E.; Marquez, I.; Lokensgard, M. E.; Rheingold, A. L.; Hecht, D. A.; Gustafson, J. L. Exploiting Atropisomerism to Increase the Target Selectivity of Kinase Inhibitors. *Angew. Chem.* **2015**, *127*, 11920–11925.

(27) Lovering, F.; Bikker, J.; Humblet, C. Escape from Flatland: Increasing Saturation as an Approach to Improving Clinical Success. *J. Med. Chem.* **2009**, *52*, 6752–6756.

(28) Salo, O. M. H.; Lahtela-Kakkonen, M.; Gynther, J.; Järvinen, T.; Poso, A. Development of a 3D Model for the Human Cannabinoid CB1 Receptor. *J. Med. Chem.* **2004**, *47*, 3048–3057.

(29) Nalbandian, C. J.; Hecht, D. E.; Gustafson, J. L. The Preorganization of Atropisomers to Increase Target Selectivity. *Synlett.* **2016**, *27*, 977–983.

(30) Yet, L. *Privileged Structures in Drug Discovery;* Wiley, **2018**.

(31) Munjal, M.; Elsohly, M. A.; Repka, M. A. Polymeric Systems for Amorphous Δ9-Tetrahydrocannabinol Produced by a Hot-Melt Method. Part II: Effect of Oxidation Mechanisms and Chemical Interactions on Stability. *J. Pharm. Sci.* **2006**, *95*, 2473–2485.

(32) Basilaia, M.; Chen, M. H.; Secka, J.; Gustafson, J. L. Atropisomerism in the Pharmaceutically Relevant Realm. *Acc. Chem. Res.* **2022**, *55*, 2904 – 2919.

(33) Minuti, L.; Temperini, A.; Ballerini, E. High-Pressure-Promoted Diels-Alder Approach to Biaryls: Application to the Synthesis of the Cannabinols Family. *J. Org. Chem.* **2012**, *77*, 7923–7931.

(34) Ashburn, B. O.; Carter, R. G. Diels–Alder Approach to Biaryls (DAB): Importance of the Ortho-Nitro Moiety in the [4 + 2] Cycloaddition. *Org. Biomol. Chem.* **2008**, *6*, 255–257.

(35) Jin, S.; Niu, Y.; Liu, C.; Zhu, L.; Li, Y.; Cui, S.; Xiong, Z.; Cheng, M.; Lin, B.; Liu, Y. Gold(I)-Initiated Cycloisomerization/Diels-Alder/Retro-Diels-Alder Cascade Strategy to Biaryls. *J. Org. Chem.* **2017**, *82*, 9066–9074.

(36) Schçnherr, H.; Cernak, T.; Profound Methyl Effects in Drug Discovery and a Call for New C – H Methylation Reactions. *Angew. Chem. Int. Ed.* **2013**, *52*, 12256–12267.
(37) Carreras, J.; Kirillova, M. S.; Echavarren, A. M. Synthesis of (−)-Cannabimovone and Structural Reassignment of Anhydrocannabimovone through Gold(I)-Catalyzed Cycloisomerization. *Angew. Chem.* **2016**, *128*, 7237–7241.
(38) Pearson, E. L.; Kanizaj, N.; Willis, A. C.; Paddon-Row, M. N.; Sherburn, Experimental and Computational Studies into an ATPH-Promoted Exo-Selective IMDA Reaction: A Short Total Synthesis of Δ9-THC. *Eur. J. Chem.* **2010**, *16*, 8280–8284.
(39) Wu, J.; Mu, R.; Sun, M.; Zhao, N.; Pan, M.; Li, H.; Dong, Y.; Sun, Z.; Bai, J.; Hu, M.; Nathan, C. F.; Javid, B.; Liu, G. Derivatives of Natural Product Agrimophol as Disruptors of Intrabacterial PH Homeostasis in Mycobacterium Tuberculosis. *ACS Infect. Dis.* **2019**, *5*, 1087–1104
(40) Pearson, E. L.; Willis, A. C.; Sherburn, M. S.; Paddon-Row, M. N. Controlling Cis/Trans-Selectivity in Intramolecular Diels–Alder Reactions of Benzo-Tethered, Ester Linked 1,3,9-Decatrienes. *Org. Biomol. Chem.* **2008**, *6*, 513–522.
(41) Gordo, J.; Avó, J.; Parola, A. J.; Lima, J. C.; Pereira, A.; Branco, P. S. Convenient Synthesis of 3-Vinyl and 3-Styryl Coumarins. *Org. Lett.* **2011**, *13*, 5112–5115.
(42) Nicolaou, K. C.; Lister, T.; Denton, R. M.; Gelin, C. F. Total Synthesis of Artochamins F, H, I, and J through Cascade Reactions. *Tetrahedron* **2008**, *64*, 4736–4757.
(43) Minami, T.; Matsumoto, Y.; Nakamura, S.; Koyanagi, S.; Yamaguchi, Masahiko. 3-Vinylcoumarins and 3-Vinylchromenes as Dienes. Application to the Synthesis of 3,4-Fused Coumarins and Chromenes. *J. Org. Chem.* **1992**, *57*, 167–173.
(44) Wertjes, W. C.; Southgate, E. H.; Sarlah, D. Recent Advances in Chemical Dearomatization of Nonactivated Arenes. *Chem. Soc. Rev.* **2018**, *47*, 7996–8017
(45) Pottie, I. R.; Nandaluru, P. R.; Benoit, W. L.; Miller, D. O.; Dawe, L. N.; Bodwell, G. J. Synthesis of 6 H-Dibenzo[b, d]Pyran-6-Ones Using the Inverse Electron Demand Diels-Alder Reaction. *J. Org. Chem.* **2011**, *76*, 9015–9030.
(46) Bonnesen, P. V.; Puckett, C. L.; Honeychuck, R. V.; Hersh, W. H. Catalysis of Diels-Alder Reactions by Low Oxidation State Transition-Metal Lewis Acids: Fact and Fiction. *J. Am. Chem. Soc.* **1989**, *111*, 6070–6081.
(47) Murakami, M.; Itami, K.; Ito, Y. Directed Intermolecular [4 + 2] Cycloaddition of Unactivated 1,3-Diene Substrates with High Regio- and Stereoselectivities. *J. Am. Chem. Soc.* **1997**, *119*, 7163–7164.
(48) Fürstner, A.; Stimson, C. C. Two Manifolds for Metal-Catalyzed Intramolecular Diels–Alder Reactions of Unactivated Alkynes. *Angew. Chem.* **2007**, *119*, 9001–9005.
(49) Wender, P. A.; Smith, T. E. Transition Metal-Catalyzed Intramolecular [4+2] Cycloadditions: Mechanistic and Synthetic Investigations. *Tetrahedron.* **1998**, *54*, 1255–1275.
(50) Wender, P. A.; Jenkins, T. E. Nickel-Catalyzed Intramolecular [4 + 2] Dienyne Cycloadditions: An Efficient New Method for the Synthesis of Polycycles Containing Cyclohexa-1,4-Dienes. *J. Am. Chem. Soc.* **1989**, *111*, 6432–6434..
(51) Jolly, R. S.; Luedtke, G.; Sheehan, D.; Livinghouse, T. Novel Cyclization Reactions on Transition-Metal Templates. The Catalysis of Intramolecular [4 + 2] Cycloadditions by Low Valent Rhodium Complexes. *J. Am. Chem. Soc.* **1990**, *112*, 4965–4966.
(52) Gilbertson, S. R.; Hoge, G. S. Rhodium Catalyzed Intramolecular [4+2] Cycloisomerization Reactions. *Tet. Lett.* **1998**, *39*, 2075–2078.
(53) Saito, A.; Ono, T.; Takahashi, A.; Taguchi, T.; Hanzawa, Y. Rh(I)-Catalyzed Mild Intramolecular [4+2] Cycloaddition Reactions of Ester-Tethered Diene-Yne Compounds. *Tet. Lett.* **2006**, *47*, 891–895.
(54) Walker, D.; Hiebert, J. D. 2,3-Dichloro-5,6-Dicyanobenzoquinone and Its Reactions. *Chem. Rev.* **2002**, *67*, 153–195.
(55) Kotha, S.; Chavan, A. S.; Goyal, D. Diversity-Oriented Approaches to Polycyclics and Bioinspired Molecules via the Diels-Alder Strategy: Green Chemistry, Synthetic Economy, and Beyond. *ACS Comb. Sci.* **2015**, *17*, 253–302.
(56) Ashburn, B. O.; Carter, R. G.; Zakharov, L. N. Synthesis of Tetra-Ortho-Substituted, Phosphorus-Containing and Carbonyl-Containing Biaryls Utilizing a Diels-Alder Approach. *J. Am. Chem. Soc.* **2007**, *129*, 9109–9116.
(57) Ashburn, B. O.; Carter, R. G. Diels–Alder Approach to Polysubstituted Biaryls: Rapid Entry to Tri- and Tetra-Ortho-Substituted Phosphorus-Containing Biaryls. *Angew. Chem. Int. Ed.* **2006**, *45*, 6737–6741.
(58) Bow, E. W.; Rimoldi, J. M. The Structure–Function Relationships of Classical Cannabinoids: CB1/CB2 Modulation. *Perspect Medicin Chem* **2016**, *8*, 17.
(59) Rhee, M.-H.; Vogel, Z.; Barg, J.; Bayewitch, M.; Levy, R.; Hanuš, L.; Breuer, A.; Mechoulam, R. Cannabinol Derivatives: Binding to Cannabinoid Receptors and Inhibition of Adenylylcyclase. *J. Med. Chem.* **1997**, 40, 3228–3233.
(60) Friesner, R. A.; Murphy, R. B.; Repasky, M. P.; Frye, L. L.; Greenwood, J. R.; Halgren, T. A.; Sanschagrin, P. C.; Mainz, D. T. Extra Precision Glide: Docking and Scoring Incorporating a Model of Hydrophobic Enclosure for Protein−Ligand Complexes. *J. Med. Chem.* **2006**, *49*, 6177–6196.